SUPERLATTICES AND MULTILAYER STRUCTURES FOR HIGH EFFICIENCY SOLAR CELLS*

M. Wagner and J. P. Leburton
Department of Electrical Engineering and
Coordinated Science Laboratory
Urbana, Illinois

Possible applications of superlattices to photovoltaic structures are discussed. A new concept based on doping superstructures (NIPI) can be exploited to significantly reduce recombination losses in III-V compound solar cells. A novel multijunction structure with lateral current transport is proposed. A computer simulation has been performed which shows that by optimizing the multilayer structure, short circuit current is substantially increased with minimum drop in open circuit voltage. An additional advantage of the structure is enhanced radiation tolerance. It is anticipated that this multilayer structure can be incorporated in multibandgap cells to achieve high efficiencies.

INTRODUCTION

Advances in epitaxial growth technologies, such as MBE and MOCVD, have made possible a large variety of new artificial materials ranging from compositional superlattices, e.g. lattice matched III-V compounds like AlGaAs/GaAs (ref. 1), to NIPI (N-doped Intrinsic P-doped Intrinsic) crystals where band structure periodicity is induced by different doping of alternate layers (ref. 2). An important advantage of these recent techniques is the ability to grow very thin layers with precise thickness and doping.

Compositional superlattices have been proposed as an alternative to homogeneous alloys for high efficiency solar cells because of lower defect densities (ref. 3). A potential difficulty though is the presence of quantized states caused by carrier confinement in the small gap layers (fig. 1.a). These states promote the capture of energetic minority carriers, enhancing recombination (ref. 4). The suitability of compositional superlattices for photovoltaic cells is therefore not apparent.

The NIPI structures, however, have a novel property of obvious interest (fig. 1.b). An indirect real space gap exists between electron states in the conduction band and hole states in the valence band (ref. 5). Photogenerated electrons and holes are spatially separated within picoseconds, allowing them almost no chance to recombine. In more familiar terms, semiconductor layer thicknesses much shorter than electron and hole minority carrier diffusion lengths yield a very high collection probability. Bulk recombination losses could seemingly be almost eliminated.

A schematic representation of a NIPI photovoltaic cell is shown in figure 2. The structure is essentially a succession of back to back pn junctions. Heavily doped contact regions, which selectively connect to either p or n layers, allow lateral transport of collected carriers. Since the junctions are connected in parallel, the open circuit voltage is determined by the layers of smallest bandgap. For this reason, only single gap NIPI cells are considered. We focus on the AlGaAs alloy system because it is currently the most promising material for high efficiency photovoltaic conversion.

Modelling

In order to evaluate the performance potential of such structures, it was decided to begin with layers sufficiently thick that the depletion region approximation would be valid. Although very thin layers reduce bulk recombination losses by allowing rapid carrier collection, a large number of layers increases the dark current. Series resistance could also become significant if the layers are so thin that adjacent space-charge regions begin to overlap.

A simulation program was developed that produces cell designs by optimizing layer thicknesses for a given set of material parameters and operating conditions. Any number of layers (greater than one) may be specified by the user. Important features of the model will be briefly described.

The p^+ and n^+ contact regions shown in figure 2 are assumed to cover a negligible fraction of the cell surface. Effects of these regions on the minority carrier distribution may then be disregarded and a one-dimensional analysis performed. To further simplify the calculation, all n-layers are assigned the same doping concentration, as are all p-layers. Future extensions of the modelling program will include individual optimization of doping for each layer.

The contributions of every layer to short circuit current, reverse saturation current, and depletion region recombination are calculated and summed. The equivalent circuit therefore consists of multiple current sources shunted by multiple diodes. We may write the resulting I-V characteristic as

$$J(V) = \sum_{m=1}^{N} J_{sc_m} - (\exp \frac{qV}{kT} - 1) \sum_{m=1}^{N} J_{o_m} - (N - 1) J_{gr} \frac{\sinh \frac{qV}{2kT}}{\frac{q}{kT}(V_b - V)} \quad (1)$$

where N is the number of layers. Depletion region recombination terms are identical for all junctions because of the stipulation that N_A and N_D are fixed. Expressions for the contributions to J_{sc} and J_o of the top and bottom layers are well known and have been presented elsewhere (ref. 6). The middle layer contributions are easily derived from the minority carrier continuity and current density equations with the boundary condition of zero excess carrier density at the depletion region edges:

$$J_{o_m} = \frac{2qD_n n_i^2}{L_n N_A} \left\{ \frac{\cosh \dfrac{t'_m}{L_n} - 1}{\sinh \dfrac{t'_m}{L_n}} \right\} \tag{2}$$

$$J_{sc_m} = \frac{qF_m \alpha L_n}{\alpha^2 L_n^2 - 1} \left\{ \alpha L_n (1 - e^{-\alpha t'_m}) - (1 + e^{-\alpha t'_m})\left(\frac{\cosh \dfrac{t'_m}{L_n} - 1}{\sinh \dfrac{t'_m}{L_n}} \right) \right\} \tag{3}$$

where t'_m is the quasi-neutral region thickness of the mth layer and F_m is the incident photon flux. Corresponding expressions for an n-doped layer are obtained simply by changing each n-subscript to a p-subscript and substituting N_D for N_A. The absorption coefficient is modelled as in reference 7.

Operation under one sun AMO conditions is assumed so J_{sc} is small enough that resistive effects may be neglected. Simulation of a NIPI cell under high concentration is substantially more complex because resistive losses cause interaction among adjacent layers. The simple parallel interconnection model no longer suffices.

A p-doped top layer was chosen to take advantage of the longer electron diffusion length. Reflection and grid coverage are assumed to cause a combined loss of 5%. The model also includes a 500 Å $Al_{0.9}Ga_{0.1}As$ window layer.

Discussion

The proposed structure is seen to enhance short circuit current at the cost of a drop in open circuit voltage (fig. 3). The fill factor also drops, but its fractional decrease is smaller than that of Voc for x > 0.2. As the number of layers is increased, bulk recombination losses become negligible and Jsc approaches a limiting value determined primarily by reflection, grid coverage, and window losses. The open circuit voltage continues to decrease, however, due to the dark current contributions of additional layers.

The trade-off between J_{sc} and V_{oc} produces a peak in efficiency at three layers (fig. 4). Note that the largest increase in efficiency over a two-layer cell occurs for x = 0.4. This is because the shorter minority carrier diffusion lengths associated with higher mole fractions of Al allow a greater margin for improved collection. The dashed curves in figure 4 indicate the performance that could be attained if the dark current contributions of the additional layers are suppressed.

The structure also exhibits higher radiation tolerance than a conventional cell. Our simulation results predict that a two-layer GaAs cell drops to 75% of its beginning-of-life efficiency after its minority carrier diffusion lengths are degraded by a factor of 3.4. However, a six-layer GaAs cell must undergo a factor of 6.5 decrease in diffusion lengths to suffer the same efficiency loss. For two-layer and six-layer $Al_{0.4}Ga_{0.6}As$ cells the degradation factors are 2.6 and 6.1 respectively. Figure 5 shows the improved performance that results from just a few additional layers when a cell has received radiation damage. Diffusion lengths were decreased by a factor of three and optimum cell designs determined for each case. The structure appears most advantageous for high mole fractions of AlAs.

CONCLUSIONS

Single bandgap multijunction structures have been studied as a means to boost the efficiency of photovoltaic cells. A computer simulation has demonstrated the potential for significant enhancement of short circuit current, especially for high gap materials with short diffusion lengths. Three or four layers appears to be optimal for highest beginning-of-life efficiency because of the dark current trade-off. An important advantage of the structure is excellent radiation tolerance. These preliminary results are encouraging, and may lead to development of more sophisticated devices where NIPI-like structures are incorporated in multibandgap solar cells.

REFERENCES

1. Dingle, R. B.: Confined Carrier Quantum States in Ultrathin Semiconductor Heterostructures. Festkorper Probleme (Advances in Solid State Physics). Edited by J. J. Queisser, Vieweg, Braunschweig 15, 21, 1975.

2. Döhler, G. H.: Doping Superlattices. J. Vac. Sci. Technol., vol. 16, 1979, 851.

3. Chaffin, R. J.; Osbourn, G. C.; Dawson, L. R.; and Biefeld, R. M.: Strained Superlattice, Quantum Well, Multijunction Photovoltaic Cell. Proc. 17th IEEE Photovoltaic Spec. Conf., Orlando, FL, 1984, Proc. p. 743.

4. Hess, K. and Holonyak, N.: Hot-electron and Phonon Effects in Layered Semiconductor Structures and Heterostructures. Comments, Solid State Phys., vol. 10, 1981, p. 67.

5. Döhler, G. H.: NIPI Doping Superlattices - Metastable Semiconductors with Tunable Properties. J. Vac. Sci. Technol. B, vol 1 (2) Apr.-June 1983, p. 278.

6. Hovel, H. J.: Solar Cells. Semiconductors and Semimetals, vol. 11, 1975.

7. Hutchby, J. A. and Fudurich, R. L.: Theoretical Analysis of $Al_xGa_{1-x}As$-GaAs Graded Band-gap Solar Cell. J. Appl. Phys., vol. 47, 1976, p. 3140
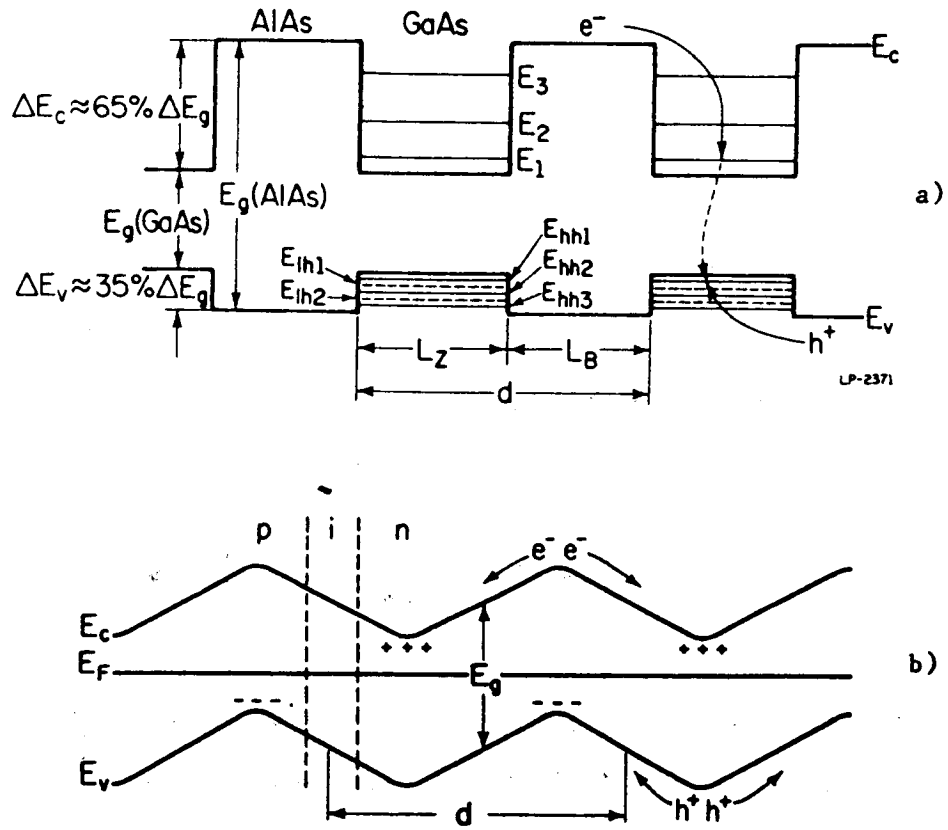
Figure 1. - Band structures of a) compositional superlattice with recombination process shown in the right-hand well and b) NIPI crystal.
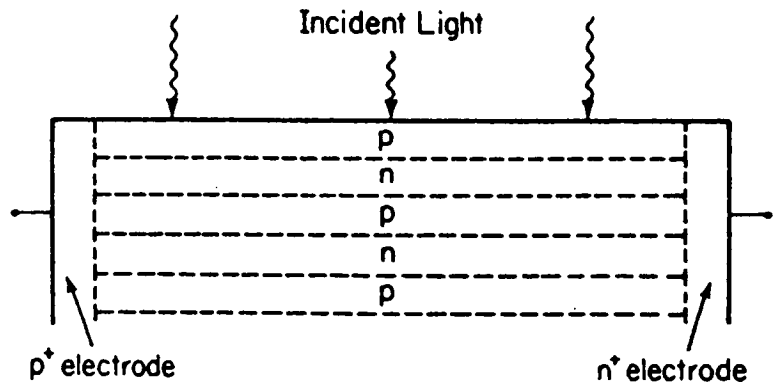

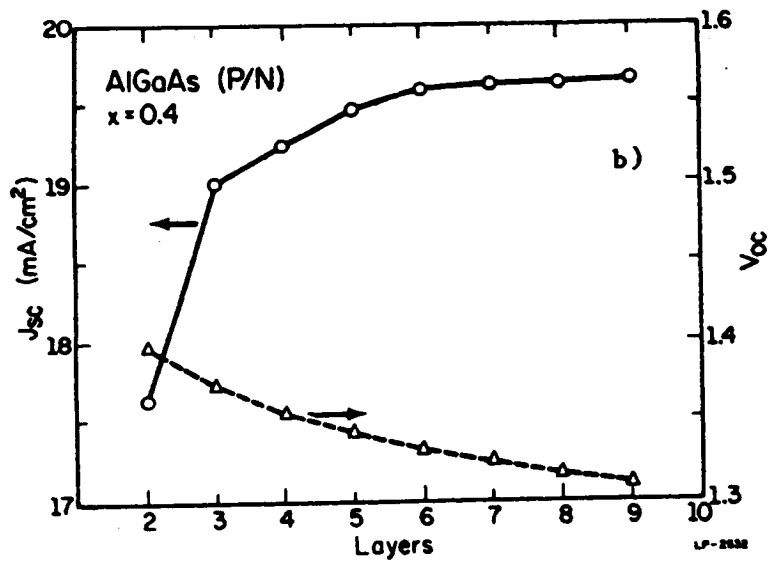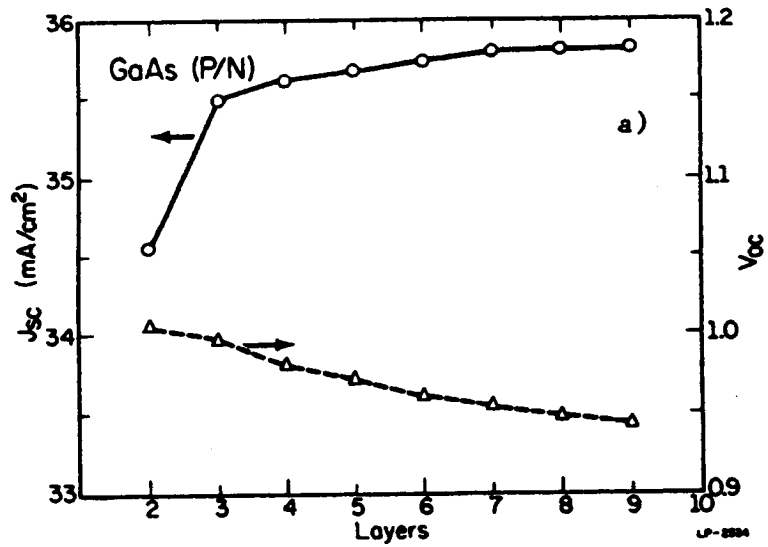Figure 2. - Schematic cross section of proposed NIPI solar cell.

Figure 3. - Trade-off between open circuit voltage and short circuit current for a) GaAs and b) $Al_{0.4}Ga_{0.6}As$ cells.
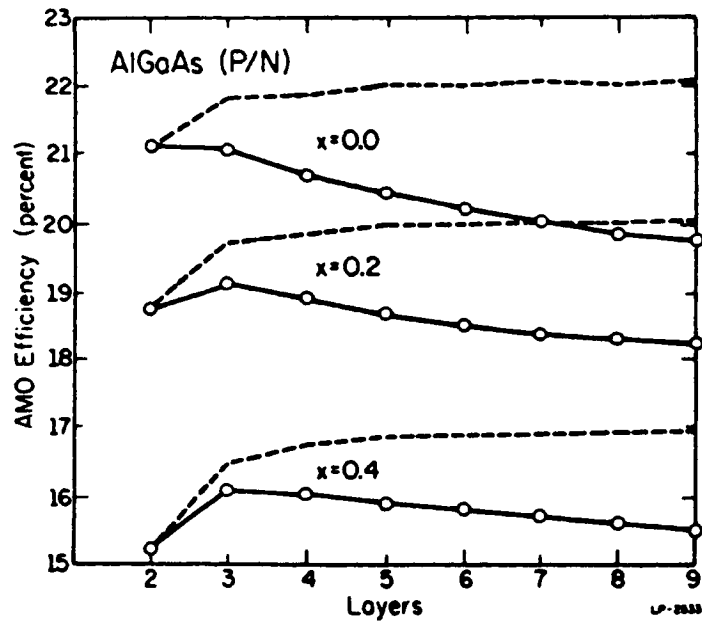
Figure 4. - Performance of cell designs optimized for one sun AMO
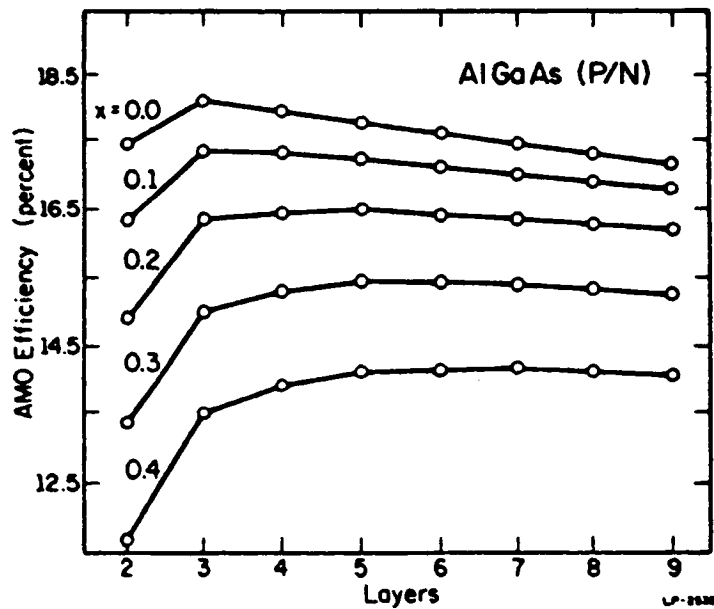operation at 300 K.

Figure 5. - Performance of radiation damaged cells optimized for
end-of-life efficiency.